1-1-1995

Spectroscopic Characteristics Of Nd3+-Doped Strontium Fluorovanadate And Their Relationship To Laser Performance

P. Hong
University of Central Florida

X. X. Zhang
University of Central Florida

R. E. Peale
University of Central Florida

H. Weldner
University of Central Florida

M. Bass
University of Central Florida

See next page for additional authors

Spectroscopic characteristics of Nd^{3+}-doped strontium fluorovanadate and their relationship to laser performance

Cite as: Journal of Applied Physics **77**, 294 (1995); https://doi.org/10.1063/1.359391
Submitted: 05 July 1994 . Accepted: 16 September 1994 . Published Online: 04 June 1998

P. Hong, X. X. Zhang, R. E. Peale, H. Weidner, M. Bass, and B. H. T. Chai

Spectroscopic characteristics of Nd^{3+}-doped strontium fluorovanadate and their relationship to laser performance

P. Hong, X. X. Zhang, R. E. Peale, H. Weidner, M. Bass, and B. H. T. Chai
CREOL—Center for Research and Education in Optics and Lasers, University of Central Florida, 12424 Research Parkway, Orlando, Florida 32826

(Received 5 July 1994; accepted for publication 16 September 1994)

High slope efficiency and low threshold laser performance have been achieved for both long pulsed and cw operation at 1.065 μm in Nd^{3+}-doped strontium fluorovanadate crystal, Nd^{3+}:$Sr_5(VO_4)_3F$, when pumped by narrow band pulsed Cr:LiSAF and cw Ti:sapphire lasers. However, there are inequivalent Nd^{3+} sites in the crystal. The absorption of Nd^{3+} ions in secondary sites, sites other than the site which contributes to lasing, may reduce the pumping efficiency and, consequently, the lasing efficiency. Strong concentration quenching of the Nd^{3+} $^4F_{3/2}$ state was also observed reducing the quantum efficiency of the laser transition from this state. © *1995 American Institute of Physics.*

I. INTRODUCTION

As efficient, high power diode lasers have become more readily available, there has been a renewed interest in the search for high efficiency and low threshold solid state laser media for diode laser pumping. The Nd^{3+}-doped apatite crystals are attractive for this purpose because they are available as large, high quality crystals and have unique spectroscopic properties appropriate for diode pumping.[1,2] This article presents the laser performance and related spectroscopic properties of a newly discovered laser crystal,[3,4] neodymium-doped strontium fluorovanadate, $Sr_5(VO_4)_3F$, or S-VAP.

S-VAP is isomorphous to calcium fluoroapatite, $Ca_5(PO_4)_3F$ or FAP,[5] which is hexagonal with a space group $P6_3/m$ and unit cell dimensions of $a_0=10.0077$ Å and $c_0=7.4342$ Å. Each unit cell contains two $Sr_5(VO_4)_3F$ molecules. Two crystallographically inequivalent Sr^{2+} sites, M_I(40%, nine-fold with C_3 symmetry) and M_{II} (60%, seven-fold with C_{1h} symmetry), exist in each unit cell. Since the M_{II} site has one F^- in coordination, it is the dominant site for rare earth substitution. An Nd^{3+} ion substitutes for an M_{II} site Sr^{2+} ion in the structure with the unbalanced charge compensated by replacing F^- ion with an C^{2-} ion.[6] A small fraction of rare earth doping may also substitute in the M_I site as will be shown by our spectroscopic data. High quality single crystals were grown by conventional Czochralski pulling in our crystal growth laboratory. The growing conditions are similar to those used to grow its isomorph, FAP.[2,7]

Laser characteristics (i.e., gain, threshold, and slope efficiency) of a material are determined by its spectroscopic properties. Using absorption, emission, excitation, and site selective spectroscopy techniques, we have identified more than two inequivalent Nd^{3+} sites in Nd:S-VAP. The energy levels of the main emitting site were determined by high resolution spectroscopic analysis. The effects of the inequivalent sites on laser performance are analyzed and the concentration dependence of the decay time of Nd^{3+} ions in S-VAP is reported.

II. SPECTROSCOPIC PROPERTIES

Spectroscopic properties of Nd^{3+}:S-VAP were studied in several samples. The Nd^{3+} doping concentration in the melts were 0.2, 1, 1.5, 2, 3, and 4 at. %, respectively, but the respective Nd^{3+} concentrations in the grown crystals were found to be 0.05, 0.26, 0.38, 0.48, 0.63, and 0.71 at. % using x-ray microprobe analysis. The distribution coefficient of Nd^{3+} ions in S-VAP crystal is different for different doping levels, decreasing as the Nd^{3+} doping level increases. That is, it is more difficult to dope Nd^{3+} into S-VAP crystal as the Nd^{3+} concentration increases.

The absorption and emission spectra were measured with a Fourier transform spectrometer. An argon ion laser and an argon ion laser pumped Ti:sapphire tunable laser were used as pumping sources in the steady state measurements. A tunable, Q-switched Cr:$LiSrAlF_6$ (Cr:LiSAF) laser was used in the luminescence dynamics measurements. The steady state luminescence measurements were made with a Si detector and the dynamic measurements employed an S_1 photomultiplier tube with nanosecond response time.

For a single site crystal two absorption lines for the $^4I_{9/2}\rightarrow{}^4F_{3/2}$ transition are expected at low temperature because of the crystal field splitting of the $^4F_{3/2}$ state of Nd^{3+} ions in crystals. Polarized transmission spectra of the $^4I_{9/2}\rightarrow{}^4F_{3/2}$ transition at 2 K are shown in Fig. 1 with a resolution of 1 cm^{-1}. Nd^{3+} ions seem to be in more than two inequivalent sites in S-VAP since at least 20 absorption lines appear for this transition. The low-energy absorption lines in the spectra are sharp while the high-energy lines appear to be broader. As the Nd^{3+} concentration increases the relative absorption coefficient of the lines in the middle of the spectrum seems to decrease as indicated in Fig. 1. The emission spectra of the $^4F_{3/2}\rightarrow{}^4I_{11/2}$ transition at 20 K when pumped by a multiline argon ion laser are shown in Fig. 2. The spectrum consists of one predominant emission line at 1.065 μm and some weaker emission lines. At this temperature, only the lower level of the $^4F_{3/2}$ manifold is populated. As a result, only six emission lines for the $^4F_{3/2}\rightarrow{}^4I_{11/2}$ transition are expected for a single site crystal. The fact that more than six emission lines are observed in Fig. 2 indicates once again the existence of more than one inequivalent site in S-VAP.

By studying the low temperature emission and absorption spectra involving transitions between the $^4F_{3/2}$ and $^4I_{9/2}$, ground state manifolds, one can identify the split sublevels

 0021-8979/95/77(1)/294/7/$6.00

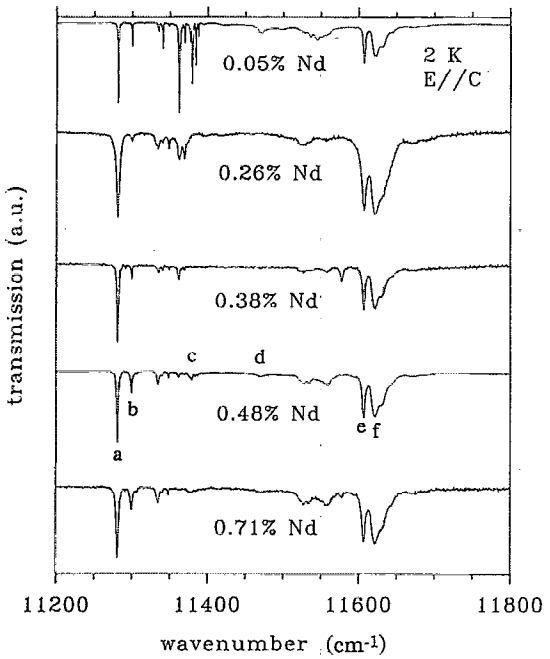

FIG. 1. π polarized transmission spectra ($^4I_{9/2} \rightarrow {}^4F_{3/2}$) of Nd^{3+}:S-VAP at 2 K for different concentrations.

of the $^4F_{3/2}$ manifold. In doing so we were able to identify those sharp lines in the lower energy side of the absorption spectra in Fig. 1 as resulting from transition to the lower sublevels of the $^4F_{3/2}$ manifold of Nd^{3+} ions in different sites and those broader lines in the higher energy side of the spectra from transition to the higher sublevels. Eleven different sites were identified in this manner and their lower sublevel positions are listed in Table I.

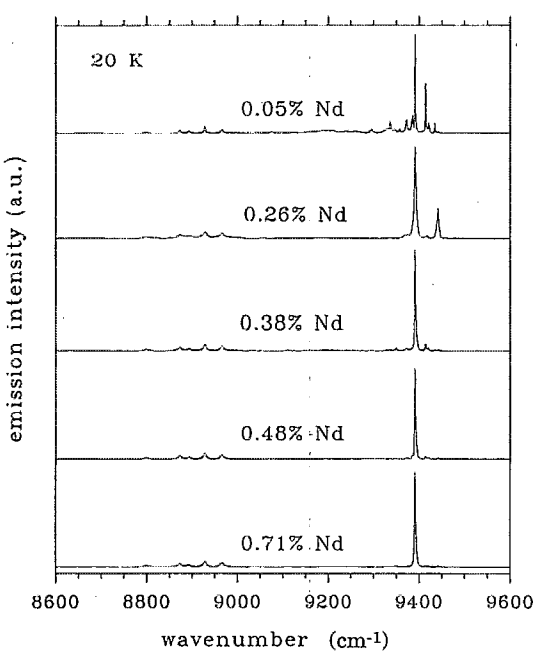

FIG. 2. Emission spectra ($^4F_{3/2} \rightarrow {}^4I_{11/2}$) of Nd^{3+}:S-VAP at 20 K for different concentrations excited by a multiline argon ion laser.

TABLE I. Energy positions of the 11 strongest inequivalent absorption lines from the lower $^4F_{3/2}$ state of Nd^{3+} ion in S-VAP at 2 K.

Spectral term	Wave number (cm^{-1})
Lower $^4F_{3/2}$	11 281, 11 300, 11 335, 11 340, 11 349, 11 362, 11 369, 11 377, 11 379, 11 384, 11 387

In order to understand the absorption and emission of these inequivalent sites, we conducted a site selective spectroscopy investigation with a 0.48% Nd^{3+}-doped S-VAP sample using a tunable Ti:sapphire laser. We selectively excited into the different $^4I_{9/2} \rightarrow {}^4F_{3/2}$ absorption lines which correspond to Nd^{3+} ions at different sites, and detected the emission spectrum of the $^4F_{3/2} \rightarrow {}^4I_{11/2}$ transition. We also measured the excitation spectra of the $^4F_{3/2} \rightarrow {}^4I_{11/2}$ emission at 1.065 μm.

As shown in Fig. 3(a), when the sample was excited at the peak of a line a (11281 cm^{-1}) in Fig. 1, only six emission lines from the $^4F_{3/2} \rightarrow {}^4I_{11/2}$ transition were observed with the strongest line centered at 1.065 μm. For excitation at

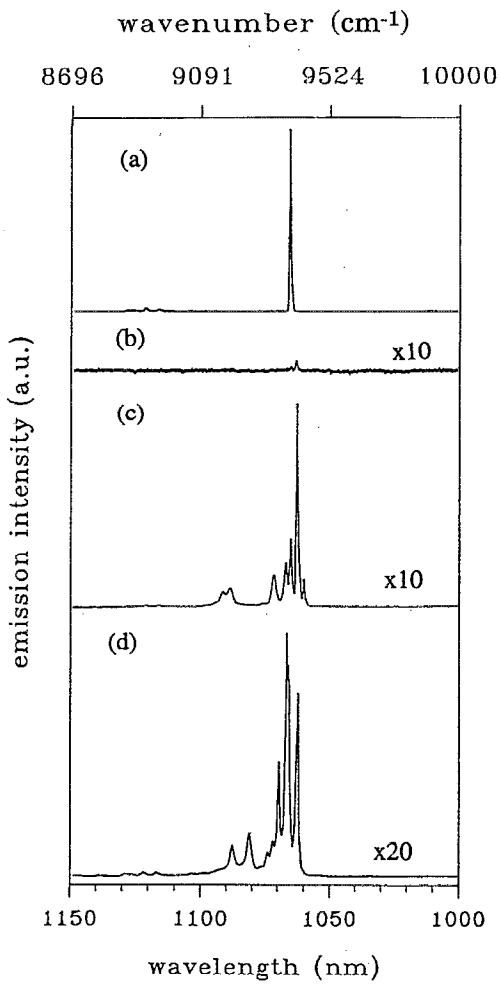

FIG. 3. Emission spectra ($^4F_{3/2} \rightarrow {}^4I_{11/2}$) of 0.48 at. % Nd^{3+}:S-VAP at 15 K when excite at (a) 11 281 cm^{-1}, (b) 11 300 cm^{-1}, (c) 11 366 cm^{-1}, and (d) 11 473 cm^{-1}.

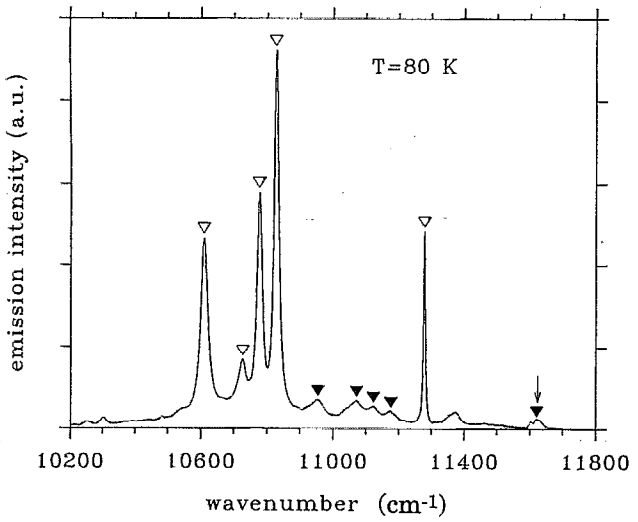

FIG. 4. 80 K emission spectra ($^4F_{3/2}\rightarrow{}^4I_{9/2}$) of 0.48 at. % Nd^{3+}:S-VAP under the excitation of a multiline argon ion laser. The hollow and filled triangles indicate the emission lines from the lower and higher sublevel of $^4F_{3/2}$, respectively. The arrow indicates the emission from lines *e* and *f* of Fig. 1.

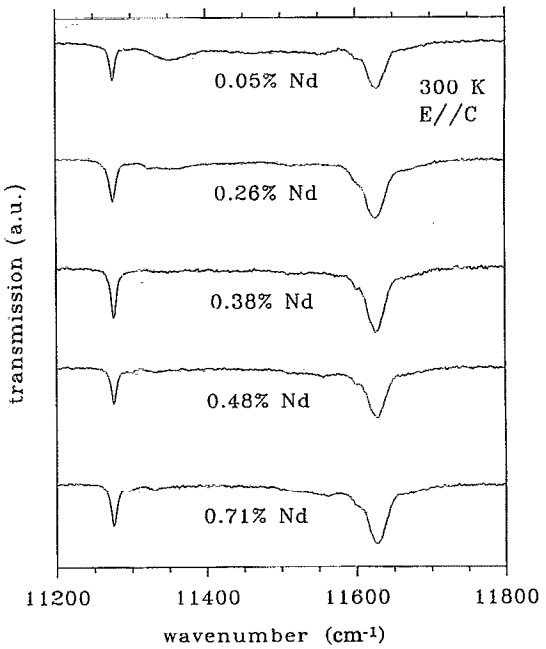

FIG. 5. Room temperature π polarized transmission spectra ($^4I_{9/2}\rightarrow{}^4F_{3/2}$) of Nd^{3+}:S-VAP with different concentrations.

lines *e* and *f*, the same spectra were obtained as when we excited line *a*, indicating that lines *e* and *f* are either of the same origin or strongly coupled. However, the energy separation between line *a* and line *f* matches the separation between the 1.065 μm emission line and its thermal replica at higher temperatures as we will see later. We therefore assign lines *a* and *f* to the split sublevels of the $^4F_{3/2}$ manifold in a particular site. We further attribute this site to the main site, M_{II} site, since its absorption and emission are the strongest observed.

Excitation at line *b* (11 300 cm^{-1}) in Fig. 1 resulted in a weak emission spectrum with the strongest line centered at 1.063 μm, as seen in Fig. 3(b). For excitation at absorption lines between line *b* and *e*, many weak emission lines, including the main emission line, were detected. The relative intensity of these weak emission lines depends on the excitation wavelength as seen in Fig. 3 curves (c) and (d). These absorption features are most probably due to ions in the M_{I} site and others that result from charge compensation, all of which we call secondary sites. The presence of the main emission line at 1.065 μm under such excitation conditions may indicate that energy transfer takes place from the secondary sites to the main site.

Absorption and emission spectra at 80 and 300 K were also measured. The absorption spectra at 80 K are almost identical to those at 2 K. Emission spectrum of the $^4F_{3/2}\rightarrow{}^4I_{9/2}$ transition at 80 K, as shown in Fig. 4, consists of the main emission lines (indicated by hollow triangles) and their thermal replicas (indicated by filled triangles). The energy difference between the emission lines from the lower $^4F_{3/2}$ state and their respective thermal replicas from the upper $^4F_{3/2}$ state matches the energy difference between absorption lines *a* and *f* shown in Fig. 1. Even though the nominal temperature is 80 K the actual temperature may be higher because the power of the argon ion laser used as excitation source was quite high (~3 W). When focused into the crystal this excitation could have heated the volume exposed.

As the temperature is raised to 300 K it appears that there are only two strong absorption lines resulting from the $^4I_{9/2}\rightarrow{}^4F_{3/2}$ transition of the main site. The other absorption lines from the secondary sites become extremely weak compared to those of the main lines, as shown in Fig. 5. The emission lines of the secondary sites are also relatively much weaker at room temperature than at 2 K as shown in Fig. 6. The sharp line emissions from the secondary sites observed at 2 K contribute to a broader band emission observed at 300 K.

The absorption lines *e* and *f* in the low temperature absorption spectrum are actually not sharp lines. They are two broad bands with strong peaks at 11 607 and 11 622 cm^{-1}, and some weak structure at the higher energy side as shown in Fig. 1. At 80 K, the whole band emits as can be seen in Fig. 4, indicated by the arrow. The excitation spectrum of the main site emission at 1.065 μm was measured at 15 K in the vicinity of lines *e* and *f*. The 1.065 μm emission intensity along with the absorbed power is plotted as a function of excitation wavelength in Fig. 7 showing that the excitation spectrum has the same structure as the absorption spectrum. It seems that even at this low temperature they are strongly coupled and the energy transfer efficiency from line *e* to the main site is about 100%.

The excitation spectrum of the main site emission at 1.065 μm was also obtained at 300 K in the 800 nm region of the $^4I_{9/2}\rightarrow{}^4F_{5/2}$, $^2H_{9/2}$ absorption and is plotted in Fig. 8. The absorption spectra for the $^4I_{9/2}\rightarrow{}^4F_{5/2}$, $^2H_{9/2}$ transition at 2 and 300 K are shown in Fig. 9 for comparison.

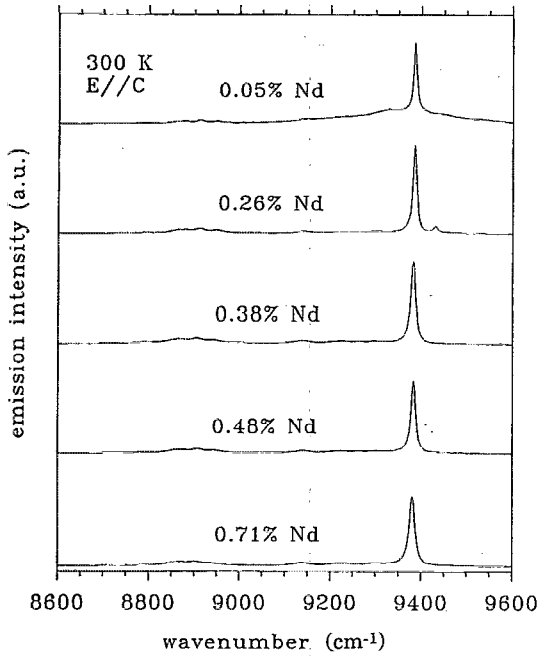

FIG. 6. Room temperature π polarized emission spectra ($^4F_{3/2} \rightarrow {}^4I_{11/2}$) of Nd^{3+}:S-VAP with different concentrations excited by a multiline argon ion laser.

Energy levels of the main site were determined from 80 K absorption and emission data and are given in Table II. The absorption line f is identified as the absorption to the upper $^4F_{3/2}$ level which is 11 624 cm^{-1} at this temperature. The Stark splitting of the $^4F_{3/2}$ level in Nd^{3+}:S-VAP is 346 cm^{-1}.

The energy levels of the secondary sites have smaller Stark splittings compared to the main site as we can see from the low temperature absorption spectra since their absorption lines lie between those of the main site. The absorption lines at the higher energy side are also broadened while the absorption lines at the lower energy side are quite sharp, which is similar to the behavior of the main site. The energy levels of the secondary sites were difficult to determine. The broadening of the absorption at higher energy side make it very difficult to correlate the upper $^4F_{3/2}$ level to the corresponding lower $^4F_{3/2}$ level for each individual site. It was not possible to separate the emissions of these secondary sites in our site selective spectroscopy experiments. This may be due to the limited spectral resolution of the excitation source and/or indicate the strong coupling between the secondary sites.

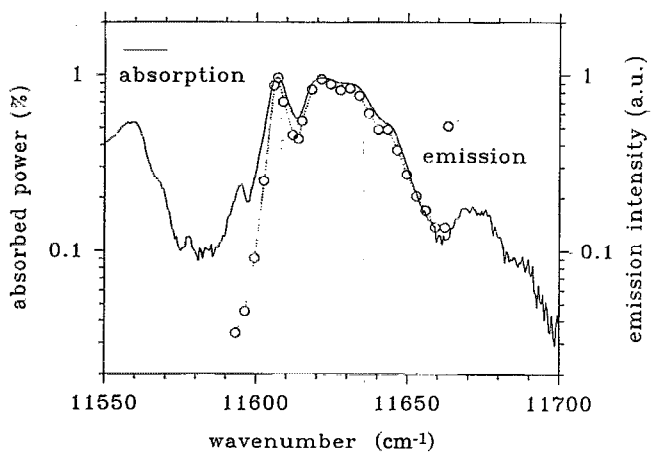

FIG. 7. Excitation spectrum of the main site emission at 1.065 μm at 15 K.

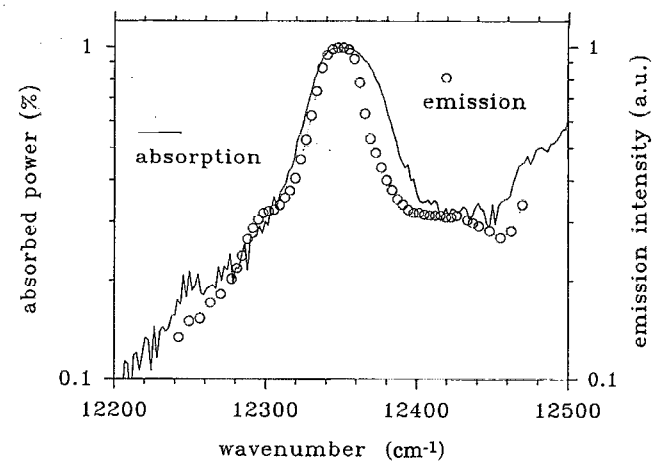

FIG. 8. Excitation spectrum of the main site emission at 1.065 μm at 300 K.

The concentration dependence of the decay time of the $^4F_{3/2}$ state was measured. The results are shown in Fig. 10. The $^4F_{3/2}$ state of Nd^{3+}:S-VAP has very strong self-absorption. To avoid the decay time lengthening due to the self-absorption,[8] luminescence decay time measurements were done with fine-ground powders of crystals. At room temperature, the luminescence decay of the $^4F_{3/2}$ state is exponential for very low Nd^{3+} concentration with a decay time of 213 μs. As the Nd^{3+} concentration is increased the

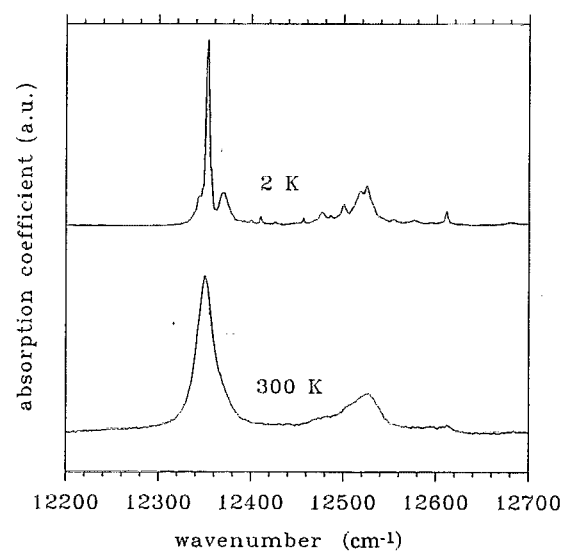

FIG. 9. π polarized transmission spectra ($^4I_{9/2} \rightarrow {}^4F_{5/2}$) of 0.48 at. % Nd^{3+}:S-VAP at 2 and 300 K.

TABLE II. Energy levels of Nd^{3+} ion in the main site of S-VAP at 80 K.

Spectral term	Wave number (cm^{-1})
$^4F_{3/2}$	11 624, 11 278
$^4I_{15/2}$	6620, 6506, 6396, 6373, 6311, 6257, 6246, 5716
$^4I_{13/2}$	4480, 4387, 4376, 4353, 4306, 4261, 3803
$^4I_{11/2}$	2484, 2410, 2391, 2357, 2319, 1889
$^4I_{9/2}$	667, 551, 499, 449, 0

decay becomes nonexponential and the decay time shorter. For nonexponential decay a mean decay time is defined as

$$\tau = \frac{1}{I(0)} \int_0^\infty I(t)dt, \tag{1}$$

where $I(0)$ and $I(t)$ are luminescence intensities at time 0 and t. The decrease of the decay time with increase in Nd^{3+} concentration indicates the existence of concentration quenching in this crystal.

III. LASER PERFORMANCE

The 0.26 at. % Nd^{3+}:S-VAP crystal was cut with flat and parallel faces containing the c axis and antireflection (AR) coated from 1.0 to 1.1 μm. It was 3.8 mm long. The laser resonator was composed of a 5 cm radius of curvature reflector (high reflectivity at 1.0–1.1 μm and high transmission at 790–810 nm) and a flat output coupler (OC) with transmission up to 5%. The pump light was focused with a 10 cm focal length lens through the HR mirror into the crystal. Both pulsed and cw laser-pump-laser experiments were performed in manners simulating diode laser pumping. Pulsed lasing was achieved by pumping with a long pulsed Cr:LiSAF laser which was tuned to the Nd^{3+}:S-VAP absorption peak at 810 nm and had a spectral bandwidth of about 1 nm. cw lasing was achieved using a cw Ti:sapphire laser tuned to 810 nm with a spectral bandwidth of about 0.1 nm. Lasing from the Nd^{3+}:S-VAP $^4F_{3/2} \rightarrow {}^4I_{11/2}$ transition at 1.065 μm is linearly polarized along the c axis (π polarization).

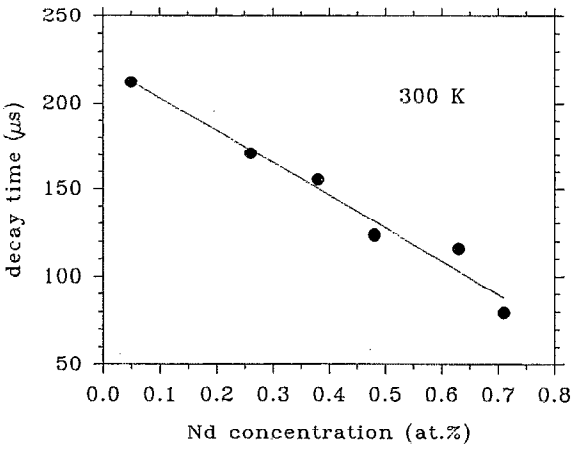

FIG. 10. Concentration dependence of the $^4F_{3/2}$ state decay time of Nd^{3+}:S-VAP at room temperature.

TABLE III. Thresholds and slope efficiencies of 0.26% Nd^{3+}:S-VAP lasing at 1.065 μm in pulsed and cw operation.

	Pulsed		cw	
T(%)	Threshold (μJ)	Slope efficiency (%)	Threshold (mW)	Slope efficiency (%)
1.2	3.6	38	5.8	29
3	5.2	59	9.4	43
5	6.0	62	13.2	49

About 85% of the long pulsed pumping energy and 98% of cw pumping power were absorbed in the laser crystal. The thresholds and slope efficiencies for both pulsed and cw operation at 1.065 μm are listed in Table III as a function of output coupling transmission. With a 5% output coupler, a slope efficiency of 62% and 49% was obtained in pulsed and cw operation, respectively. Higher slope efficiency is expected with a higher transmission output coupler.[3,4]

A 1.3 mm 0.65 at. % Nd^{3+}-doped S-VAP crystal was also tested for laser performance in the same cavity. A slope efficiency of only 22% was obtained with a 5% output coupler in cw operation. The thresholds and slope efficiencies of this crystal in pulsed and cw operation are listed in Table IV as a function of output coupler transmission.

IV. DISCUSSION

The main site, M_{II}, for the Nd^{3+} ion in S-VAP is the site of the lasing ions. Room-temperature emissions originate principally from ions in the M_{II} site while the other lines seen at 20 K contribute to a broad emission band (see Fig. 6). The peak absorption cross section of the $^4I_{9/2} \rightarrow {}^4F_{5/2}, {}^2H_{9/2}$ transition at 809.6 nm is 3×10^{-19} cm^2 with a linewidth around 2 nm. The emission from the $^4F_{3/2} \rightarrow {}^4I_{11/2}$ transmission of the main site is highly polarized in π polarization ($E//c$) and has an emission cross section[3] of 5×10^{-19} cm^{-2}. The emission is dominated by one single narrow emission line at 1.065 μm having a line width of 1.2 nm.

As we can see in Fig. 9 the absorption spectra which would enable diode laser pumped lasing at 300 K actually contains absorptions of the main site and the secondary sites, i.e., the wide absorption width at room temperature is partly due to absorption by Nd^{3+} ions in the secondary sites. It is

TABLE IV. Thresholds and slope efficiencies of 0.65% Nd^{3+}:S-VAP lasing at 1.065 μm in pulsed and cw operation.

	Pulsed		cw	
T(%)	Threshold (μJ)	Slope efficiency (%)	Threshold (mW)	Slope efficiency (%)
1.2	5.0	23	9.5	11
3	10.0	36	16.4	18
5	13.0	46	19.8	22

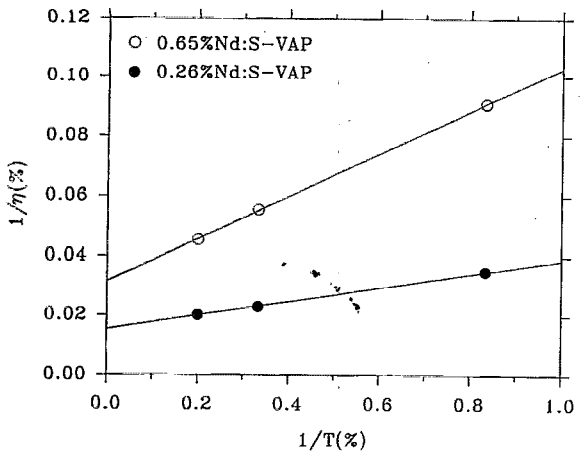

FIG. 11. Inverse slope efficiency versus inverse output coupling for 0.26% Nd^{3+} and 0.65% Nd^{3+}-doped S-VAP laser crystals when lasing at 1.065 μm.

clear that the absorption of the secondary sites, which is on the sides of the absorption band, does not contribute to the 1.065 μm emission as efficiently as the main site absorption, as demonstrated in the excitation spectrum of Fig. 8. In the other words, the absorption of the secondary sites reduces the pump efficiency. Therefore, this crystal is not appropriate for broadband pumping. The wide absorption width of Nd^{3+}-doped S-VAP (about 2 nm) is not an advantage for this crystal since it results from contributions from inequivalent sites. It is an extreme case of inhomogeneous broadening.

In a cw laser-pumped laser experiment the slope efficiency obtained depends, under the condition of 100% pump efficiency, on the quantum efficiency, the pump and lasing wavelengths, and the loss present in the laser material in the following relation:[2]

$$\eta=(\eta_q\lambda_p/\lambda_l)T/(T+L), \tag{2}$$

where η_q is the quantum efficiency λ_p and λ_l are the pump and lasing wavelengths, T is the output coupling, and L is the cavity loss. $1/\eta$ is linearly dependent on $1/T$, which can be seen if Eq. (2) is inverted to give,

$$1/\eta=1/\eta_0+(L/\eta_0)1/T, \tag{3}$$

where

$$\eta_0=\eta_q\lambda_p/\lambda_l \tag{4}$$

is the intrinsic slope efficiency (i.e., is the slope efficiency when there is no loss present). For Nd^{3+}-doped S-VAP the pumping and lasing wavelengths are 810 and 1065 nm, respectively. Therefore, we have $\lambda_p/\lambda_l=76\%$, and the intrinsic slope efficiency is proportional to the quantum efficiency.[2]

The loss present in laser performance can be derived from the slope efficiency obtained in the cw laser-pumped laser experiment using Eq. (3). The plot of the inverse output coupling versus the inverse slope efficiency for 0.26 at. % Nd^{3+}-doped S-VAP, Fig. 11, gives an intrinsic slope efficiency of 67% and a passive loss of 2.0% cm^{-1} for cw operation. The plot of the inverse output coupling against the versus slope efficiency for 0.65 at. % Nd^{3+}-doped S-VAP crystal is also given in Fig. 11. An intrinsic slope efficiency of 32% and a passive loss of 8.9% cm^{-1} is obtained.

In the presence of concentration quenching the quantum efficiency is equal to the ratio of the mean decay time to the radiative decay time. For 0.26 at. % Nd^{3+}-doped S-VAP, the mean decay time of the 1.065 μm emission is 171 μs. Then the quantum efficiency is equal to 80%. But for 0.65 at. % Nd^{3+}-doped S-VAP the mean decay time is only 128 μs, which gives a quantum efficiency of 60%. Lower quantum efficiency will result in lower intrinsic slope efficiency and, consequently, lower measured slope efficiency.[2] Therefore, the slope efficiency of the 0.65 at. % Nd^{3+}-doped S-VAP is expected to be lower than that of the 0.26 at. % Nd^{3+}-doped S-VAP. That partially explains the lower slope efficiency we obtained form the 0.65 at. % crystal. Also the crystal quality of the high concentration sample is not as good as the low concentration one, which results in higher passive loss and contributes to the decreased slope efficiency.

V. SUMMARY

In summary, we have investigated the spectroscopic properties and laser performance of the newly discovered laser crystal, Nd^{3+}-doped $Sr_5(VO_4)_3F$. Detailed spectroscopic studies show that there exist at least 11 spectroscopically different Nd^{3+} sites although there are only two inequivalent crystallographic sites ($M_{\rm I}$ and $M_{\rm II}$ sites) where Nd^{3+} ions can reside in this crystal. The strongest absorption and emission observed result from the transition of Nd^{3+} ions in $M_{\rm II}$ sites, the most common or main site. Nd^{3+} ions in this site are responsible for the lasing action. The multisite nature is believed to result from the doping of Nd^{3+} ions in $M_{\rm I}$ sites and the inequivalent charge compensation induced by this doping. Although the site selective spectroscopy indicates that there is energy transfer from the secondary sites to the main site, the excitation spectrum taken in the vicinity of diode laser pumping wavelength shows that this transfer efficiency is quite low. The pump efficiency, and thus the lasing efficiency, will be reduced by the absorption of the secondary sites in the vicinity of the diode laser wavelength. Therefore, excellent laser performance is not expected for broadband pumping although high slope efficiency and low threshold laser performance of both pulsed and cw operation in low Nd^{3+} concentration $Sr_5(VO_4)_3F$ crystal at 1.065 μm have been achieved when pumped with narrow band pulsed Cr:LiSAF and cw Ti:sapphire lasers. Concentration quenching was observed in high Nd^{3+} concentration crystals, and it is shown to degrade the laser performance in this crystal.

ACKNOWLEDGMENTS

This work was supported by the Advanced Research Projects Agency (ARPA) and by the Florida High Technology and Industry Council. The fabrication of crystals and the mirror coatings supplied by Lightning Optical Corp. is gratefully appreciated.

[1] X. X. Zhang, P. Hong, G. Loutts, J. Lefaucheur, M. Bass, and B. H. T. Chai, Appl. Phys. Lett. **64**, 3205 (1994).
[2] X. X. Zhang, G. B. Loutts, M. Bass, and B. H. T. Chai, Appl. Phys. Lett. **64**, 10 (1994).

[3] S. A. Payne, B. H. T. Chai, W. L. Kway, L. D. DeLoach, L. K. Smith, G. Lutts, R. Peale, X. X. Zhang, G. D. Wilke, and W. F. Krupke, Conference on Lasers and Electro-Optics (CLEO), Baltimore, 1993, postdeadline paper CPD12.
[4] B. H. T. Chai, G. Lutts, R. Peale, X. X. Zhang, S. A. Payne, W. F. Krupke, L. D. DeLoach, and L. K. Smith, Opt. Lett. (to be published).
[5] D. A. Grisafe and F. A. Hummel, J. Solid State Chem. **2**, 160 (1970).
[6] R. C. Ohlmann, K. B. Steinbruegge, and R. Mazelsky, Appl. Opt. **7**, 905 (1968).
[7] G. B. Loutts and B. H. T. Chai, Proc. SPIE **1863**, 31 (1993).
[8] X. X. Zhang, P. Hong, B. Di Bartolo, C. W. Struck, and M. Bass, J. Phys.:Condens. Matter **6**, 4661 (1994).